Journal of Molecular Structure 1321 (2025) 139999

Contents lists available at ScienceDirect

Journal of Molecular Structure

journal homepage: www.elsevier.com/locate/molstr

Schiff base substituted non-peripheral symmetrical cupper, cobalt, and manganese phthalocyanines: Synthesis, design, electrochemistry, and spectroelectrochemistry

Halise Yalazan [a], Zehra Kurtuluş [b], Atıf Koca [b], Halit Kantekin [a,*]

[a] Faculty of Sciences, Department of Chemistry, Karadeniz Technical University, Trabzon, 61080, Türkiye
[b] Engineering Faculty, Department of Chemical Engineering, Marmara University, İstanbul, Türkiye

ARTICLE INFO

Keywords:
Electrochemistry
Phthalocyanines
Schiff bases
Spectroelectrochemistry

ABSTRACT

Novel Co^{II} (**nANTH—CoPc**), Cu^{II} (**nANTH—CuPc**), and $Mn^{III}Cl$ (**nANTH-MnClPc**) phthalocyanines were obtained by substituting the 3-(4-((1,5-dimethyl-3-oxo-2-phenyl-2,3-dihydro-1*H*-pyrazol-4-ylimino)methyl)phenoxy) Schiff base compound (**nANTH—OH**) obtained by the acid-catalyzed condensation reaction of 4-aminoantipyrine and 4-hydroxybenzaldehyde at non-peripheral positions. By using various spectroscopic techniques, (NMR, MALDI-TOF, FT-IR, and UV–Vis), the structures of green-colored phthalocyanine compounds and precursor phthalonitrile compounds were identified. The electrochemical responses of cobalt (II) (**nANTH—CoPc**), cupper (II) (**nANTH—CuPc**), and manganese (III) (**nANTH-MnClPc**) phthalocyanines were determined, and their redox responses were analyzed based on the different metal centers. The results indicated that using redox-active Co^{2+} and Mn^{3+} cations instead of Cu^{2+}enhanced the redox richness of the complexes due to the observation of extra metal-based electron transfer reactions in addition to the Pc-based ones. *In-situ* spectroelectrochemical analyses of the complexes were used to support the peak assignments of the redox processes and the spectrum and color of the electrogenerated species during the redox reactions. Supported these redox mechanisms. Multi-electron transfer processes and distinct color changes during these processes indicate the possible usage of these complexes in various electrochemical and opto-electrochemical processes. Metal-based electron transfer reactions illustrated different spectral changes than those of the Pc-based ones, and these spectral changes significantly differed the color of the anionic and cationic species.

1. Introduction

Recent years have witnessed significant advancements in the field of electrochemical organic synthesis. Organic synthesis is one of the most potential fields for electrochemical methodology development, as it can facilitate the simplification of synthetic pathways. As such, there has already been a significant rise in the finding of novel compounds based on phthalocyanines (Pcs). A significant strategy for using phthalocyanines in the realm of electrochemistry is the design and construction of novel phthalocyanines that include appropriate metal ions and substituted groups inside the same molecule [1–3].

Aromatic macrocyclic compounds, metallophthalocyanines (MPcs), possess an 18 π-electron system and have extensive uses in multiple fields, including enzyme inhibition [4–6], photocatalytic [7–9], sensor [10,11], photovoltaic [12,13], solar cells [14–16], and photodynamic therapy [17–19]. In addition, metallophthalocyanines have been used in various electrochemical technologies, such as electro-catalytic, electro-sensing, and electro-chromic fields, due to their rich redox properties [20–22]. The redox activities of MPcs are assigned to the Pc ring, metal center, and/or the substituents. The Pc ring can illustrate up to four reduction and two oxidation processes due to the conjugated 18 π electrons of the Pc ring. Additionally, redox-active metal centers and redox-active substituents can cause extra electron transfer reactions in addition to those of the Pc ring [23–25].

Pcs with redox-active metal centers (such as Cr, Co, Fe, Mn, etc.) are particularly significant due to their electrochemical characteristics. Of these, the corresponding metallophthalocyanines (MPcs) with oxidation states ranging from Mn^{+} to Mn^{4+} and from Co^{1+} to Co^{3+} exhibit promising electrochemical capabilities owing to the electroactive nature of the two essential metals, Mn and Co [26,27]. Although the synthesis

* Corresponding author.
E-mail address: halit@ktu.edu.tr (H. Kantekin).

https://doi.org/10.1016/j.molstruc.2024.139999
Received 15 July 2024; Received in revised form 4 September 2024; Accepted 7 September 2024
Available online 12 September 2024

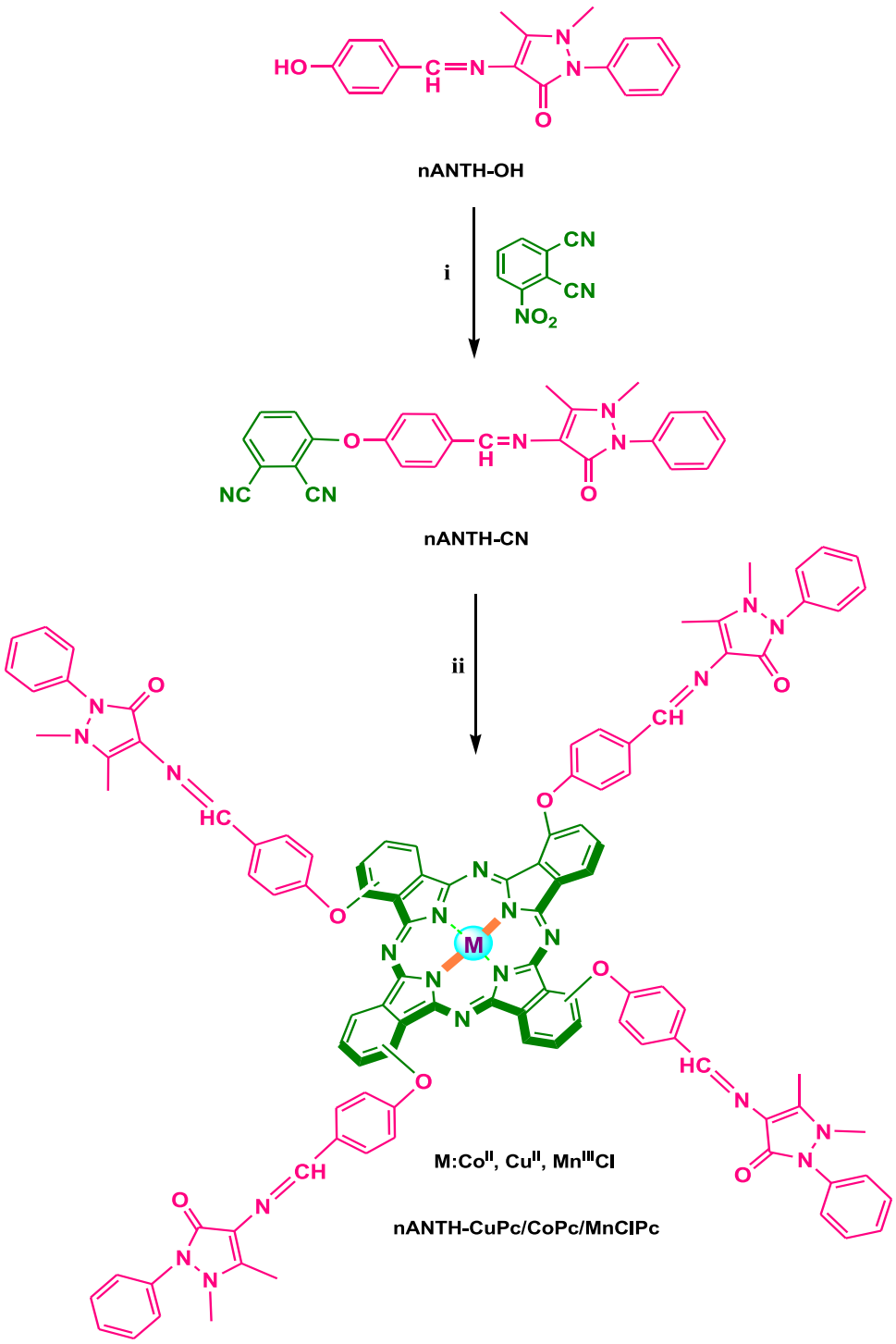

Scheme 1. Phthalonitrile compound (**nANTH—CN**) and Schiff base substituted non-peripheral symmetrical cupper (**nANTH—CuPc**), cobalt (**nANTH—CoPc**), and manganese (**nANTH-MnClPc**) phthalocyanines. (i) dry DMF, N_2, 55 °C, anhydrous K_2CO_3 **(ii)** $CoCl_2$, $CuCl_2$, and $MnCl_2$, N_2, DBU, n-penthanol, 138 °C. M: Co^{II}, Cu^{II}, $Mn^{III}Cl$.

and electrochemistry of many MPcs have been documented in the literature, the majority of these complexes—such as Co^{II}, Zn^{II}, Cu^{II}, and Ni^{II}—feature a $M^{II}Pc$ core because of their easy synthesis, high yield, and simplicity of purification [28,29]. Due to their redox richness, MPcs featuring more oxidized metal centers are rare and have more application potential [30–35]. Since the metal center of $Mn^{III}ClPc$ has a 3+ oxidation state, the metal center has an axial ligand. An axial ligand's capacity to bind to the central metal ion of MPc allows it to be used as a potential functional material for applications such as electrochemical sensing and electrocatalytic reduction/oxidation. The target species and MPcs' electron transport characteristics are impacted by this type of complex binding of the target species to the axial location of the metal center [36].

There are many papers on the electrochemistry and spectroelectrochemistry of different metal phthalocyanines including Co, Cu and Mn metal centers. It is known that redox properties of MPcs can be altered by changing the metal centers and substituent environments. Type, number and position of substituents influence the solubility and

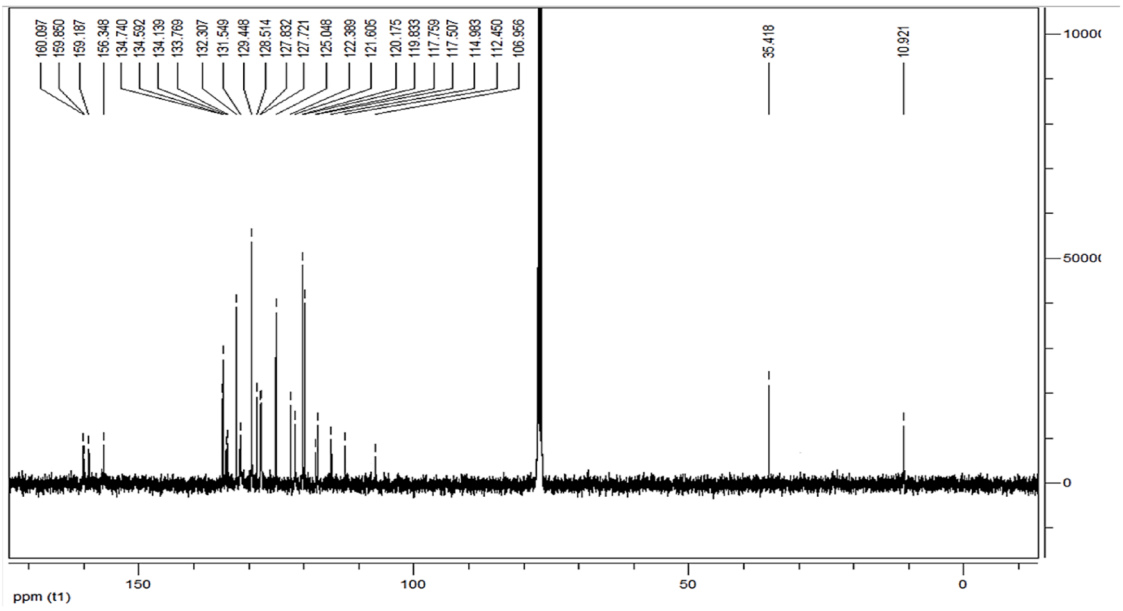

Fig. 1. ^{13}C NMR spectrum of **nANTH—CN**.

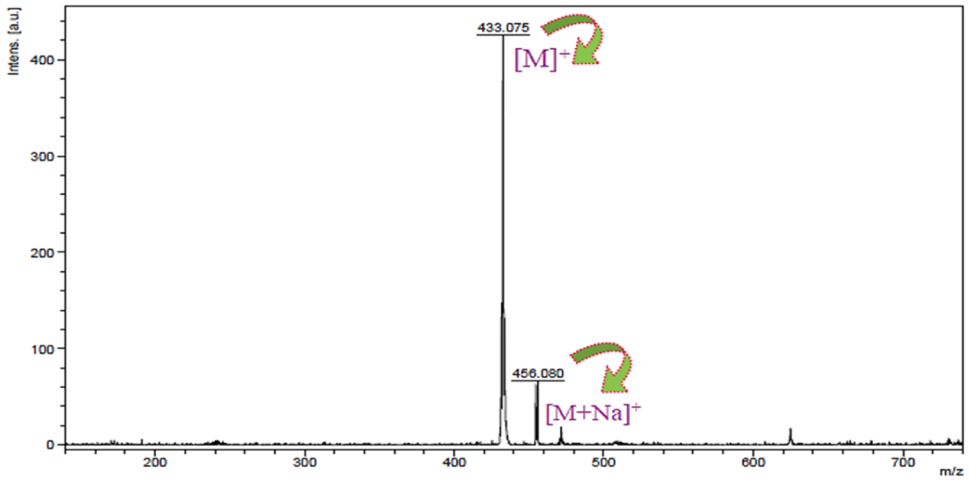

Fig. 2. Mass spectrum of **nANTH—CN**.

aggregation properties of the complexes which influence their electrochemical features [36]. Additionally, electron withdrawing/releasing behaviors of the substituents affects the positions of these complexes. Thus it is important to determine the electrochemistry and spectroelectrochemistry of newly synthesized metal phthalocyanines to predict their possible applications in different fields. The nature, kind, and electron transfer capabilities of the metal or substituents, as well as their solubility and aggregation characteristics, determine the potential applications of Pcs. By attaching bulky groups in the right locations and adding the appropriate metal, Pcs with rich redox characteristics and high solubility may be designed [3]. The electrochemical reactions of the Pc ring and metal core are known to be more impacted by non-peripherally substituted moieties than by peripheral substitution. For instance, because of the substituents' steric influence and/or electron-releasing capacity, non-peripheral substitutions hinder the interaction of the core metal with molecular oxygen [33].

Schiff bases, which are structures with the imine bond N═CH-, are commonly recognized. They are created by condensing primary amines with carbonyl groups that are active, such as aldehydes or ketones, and then removing the water. The availability of donor lone electron pairs on the nitrogen atom, conjugation ability, and the capacity to offer a significant degree of conformational flexibility needed by supramolecular chemistry are the benefits of the imine moiety [37]. In this study, Schiff base compounds designed as a substituent group for the Pc ring have wide applications in medicine and biological processes, and there are a limited number of studies examining their electrochemical properties. It is well known that redox responses of MPc are significantly influenced with the substituents in addition to the effects of metal centers [38–40], thus it is important to determine the redox features of newly synthesized **nANTH—CoPc, nANTH—CuPc**, and **nANTH-MnClPc** complexes in order to predict their possible applications in different areas.

Taking all these features into consideration, the synthesis of Schiff base-substituted non-peripheral **nANTH—CoPc, nANTH—CuPc**, and **nANTH-MnClPc** was designed in this study. To predict possible application fields of the newly synthesized phthalocyanines, detailed electrochemical properties should be determined. For this purpose, we have investigated the voltammetric and spectroelectrochemical responses of **nANTH—CoPc, nANTH—CuPc**, and **nANTH-MnClPc**.

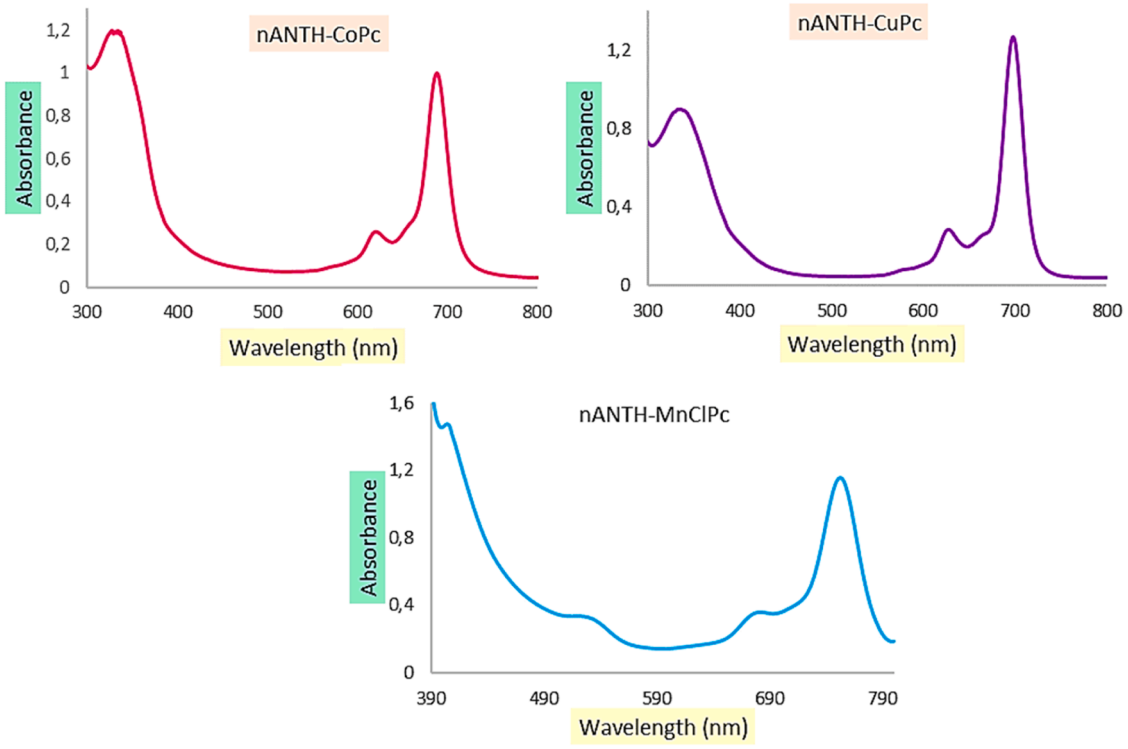

Fig. 3. UV–Vis spectra of **nANTH—Co/Cu/MnClPc**.

Table 1
Electrochemical data of the complexes in DMSO/TBAP solution. All potentials were given versus Ag/AgCl.

	$E_{1/2}$ (V) of Redox Processes					
Complexes	R_1	R_2	R_3	O_1	O_2	Refs.
nANTH—CuPc	−0.63	−1.02	−1.46	0.97 (1.02)[a]	1.43	tw
nANTH-CoPc	−0.32	−067	−1.20	0.31	0.94 (1.19)[b]	tw
nANTH-MnClPc	0.24	−0.67	−1.25	0.96	1.16	tw
CoPc	−0.48	−1.29	−1.92	0.30	0.91	[65]
CoPc	−0.38	−1.30	–	0.39	–	[49]
CoTMPyrPc	−0.50	−1.34	−1.93	0.47	1.00	[66]
CoTMPyrPc	−0.26	−1.25	−1.84	0.52	1.00	[58]
CuPc(mpt)	−0.95	−1.21	−1.88	0.58	1.30	[67]
CuPc	−0.70	−1.02	–	0.68	1.13	[58]
CuPc	−0.73	−1.08	−1.64	–	–	[49]
MnClPc	−0.30	−0.90	−1.36	0.38 (0.51)	0.88	[65]
MnClPc	−0.08	−0.84	–	0.30	0.87	[68]
MnTMPyrPc	−0.06	−0.68	−1.19	–	–	[66]
MnClPc(m)	−0.23	−0.80	−1.04	–	–	[69]

[a] : CoPc illustrated O_3 at 0.90 V and O_4 at1.20 V in addition to O_1 and O_2 in DMSO/TBAP electrolyte.

2. Experimental

Supplementary information is provided, including the materials, equipment, and electrochemical and *in situ* spectroelectrochemical measurements of the phthalocyanines.

2.1. Synthesis

2.1.1. 3-(4-((1,5-dimethyl-3-oxo-2-phenyl-2,3-dihydro-1H-pyrazol-4-ylimino)methyl)phenoxy) phthalonitrile (*nANTH—CN*)

In 20 mL of dry dimethyl formamide (DMF), the yellow Schiff base compound (0.46 g, 1.50 mmol) (**nANTH—OH**) was dissolved, and then 3-nitrophthalonitrile was added to the reaction content. Anhydrous K_2CO_3 (0.62 g, 4.50 mmol) began to be added to the reaction content in parts as soon as the temperature reached 50 °C. With the addition of K_2CO_3, the color of the reaction mixture changed from yellow to dark brown. For ninety hours, the reaction mixture with a dark brown color was stirred at 55 °C in an atmosphere of nitrogen. Following the pouring of this mixture into about 100 g of ice, the product precipitated and was filtrated. Using a column containing alumina and a chloroform solvent, the resultant product was purified using column chromatography. A yellow solid known as phthalonitrile compound (**nANTH—CN**) was produced.

Yields: 55% (0.36 g). Melting point: 248−250 °C. FT–IR (ATR), υ_{max} (cm^{-1}): 3088 (Ar−H), 2930−2853 (Aliph. C−H), 2231 (C≡N), 1682 (C=O), 1649 (C=N), 1574, 1497, 1455, 1358, 1269, 1198, 1133, 1099, 984, 852, 769. ^{1}H NMR (DMSO-d_6), (δ:ppm): 9.68 (s, 1H, C=N), 8.09 (d, 1H, Ar−H), 7.91 (d, 1H, Ar−H), 7.63−7.50 (m, 1H, Ar−H), 7.44 (t, 2H, Ar−H), 7.32 (d, 2H, Ar−H), 7.19 (s, 1H, Ar−H), 7.14 (d, 2H, Ar−H), 7.09 (d, 2H, Ar−H), 3.16 (s, 3H, N−CH_3), 2.57 (s, 3H, CH_3). ^{13}C NMR ($CDCl_3$), (δ:ppm): 160.09 (C=N), 159.85, 159.18, 156.35, 134.74, 134.59, 134.14, 133.77, 132.31, 131.55, 129.45, 128.51, 127.83, 127.72, 125.05, 122.39, 121.60, 120.17, 119.83, 117.76 (C≡N), 117.51 (C≡N), 114.98, 112.45, 106.96, 35.42 (N−CH_3), 10.92 (CH_3). MS (MALDI–TOF) *m/z*: Calculated: 433.46; found 433.07 as $[M]^+$ for $C_{26}H_{19}N_5O_2$.

2.1.2. Schiff base substituted non-peripheral metallated phthalocyanines (*nANTH—Co/Cu/MnClPc*)

Following the dissolution of the phthalonitrile compound (**nANTH—CN**) (0.1 g, 0.23 mmol) in n-pentanol (5 mL), anhydrous metal salt ($CoCl_2$ (0.015 g, 0.12 mmol) or $CuCl_2$ (0.015 g, 0.12 mmol) or $MnCl_2$ (0.014 g, 0.12 mmol)) and 1,8-diazabicyclo[5.4.0]undec-7-ene (DBU) (8 drops) were added. When metal salt and DBU were added, the reaction content's color changed from light yellow to dark green. The mixture with a green color was mixed for 19 h at 138 °C in an atmosphere of nitrogen, and then the product was filtered after being precipitated by the addition of ethyl alcohol (20 mL). Using an alumina-loaded column and a solvent system consisting of chloroform (5 mL):

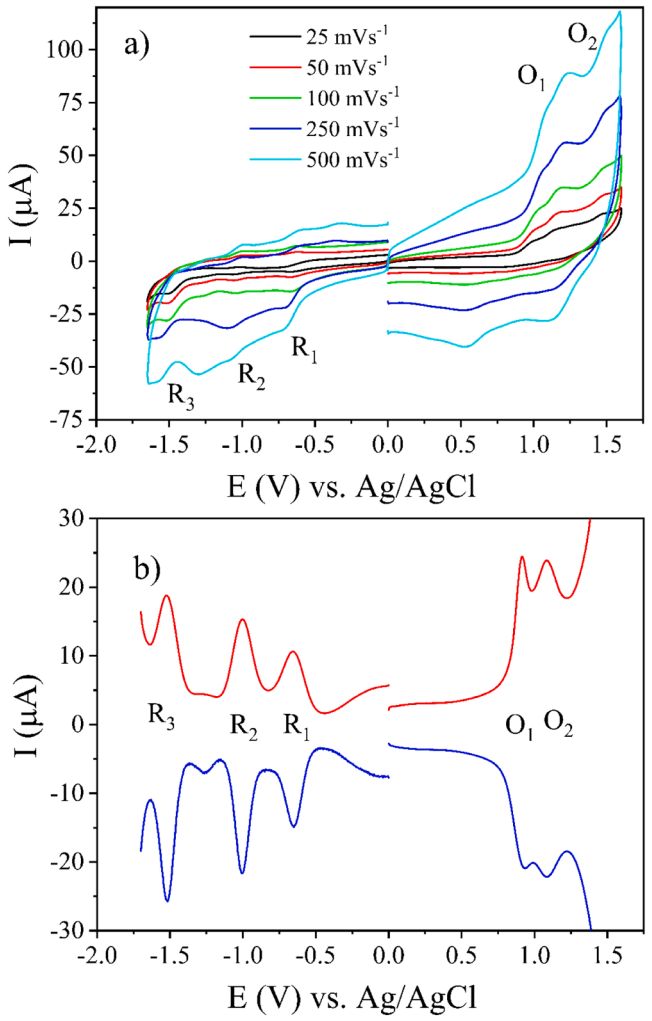

Fig. 4. CVs and SWVs of **nANTH—CuPc** (5.0×10^{-4} mol.dm^{-3}) recorded at various scan rates on a GCE working electrode in DMSO/TBAP.

ethyl alcohol (2 drops) (for all compounds), the green solid was purified by column chromatography. The corresponding title products were produced as solids with colors of turquoise green, dark blue, and brown-green for $Co^{II}Pc$ (**nANTH—CoPc**), $Cu^{II}Pc$ (**nANTH—CuPc**), and $Mn^{III}ClPc$ (**nANTH-MnClPc**), respectively.

*2.1.2.1. 1(4),8(11),15(18),22(25)-[4-((1,5-dimethyl-3-oxo-2-phenyl-2,3-dihydro-1H-pyrazol-4-ylimino)methyl)phenoxy)] phthalocyaninato cobalt (II) (**nANTH—CoPc**).* Yields: 26% (26 mg). Melting point >300 °C. FT–IR (ATR), υ_{max} (cm^{-1}): 3060 (Ar–H), 2926–2857 (Aliph. C–H), 1713, 1650, 1590, 1499, 1331, 1244, 1211, 1134, 1093, 978, 833. UV–Vis ($CHCl_3$), λ_{max}, nm (logε): 690 (4.99), 620 (4.42), 337 (5.08). MS (MALDI–TOF) *m/z*: Calculated: 1792.78; found 1793.97 as $[M+H]^+$ for $C_{104}H_{76}N_{20}O_8Co$.

*2.1.2.2. 1(4),8(11),15(18),22(25)-[4-((1,5-dimethyl-3-oxo-2-phenyl-2,3-dihydro-1H-pyrazol-4-ylimino)methyl)phenoxy)] phthalocyaninato cupper (II) (**nANTH—CuPc**).* Yields: 29 % (29 mg). Melting point >300 °C. FT–IR (ATR), υ_{max} (cm^{-1}): 3063 (Ar–H), 2926–2856 (Aliph. C–H), 1713, 1645, 1590, 1477, 1338, 1245, 1156, 1091, 976, 833. UV–Vis ($CHCl_3$), λ_{max}, nm (logε): 698 (5.10), 627 (4.46), 335 (4.95). MS (MALDI–TOF) *m/z*: Calculated: 1797.39; found 1797.85 as $[M]^+$for $C_{104}H_{76}N_{20}O_8Cu$.

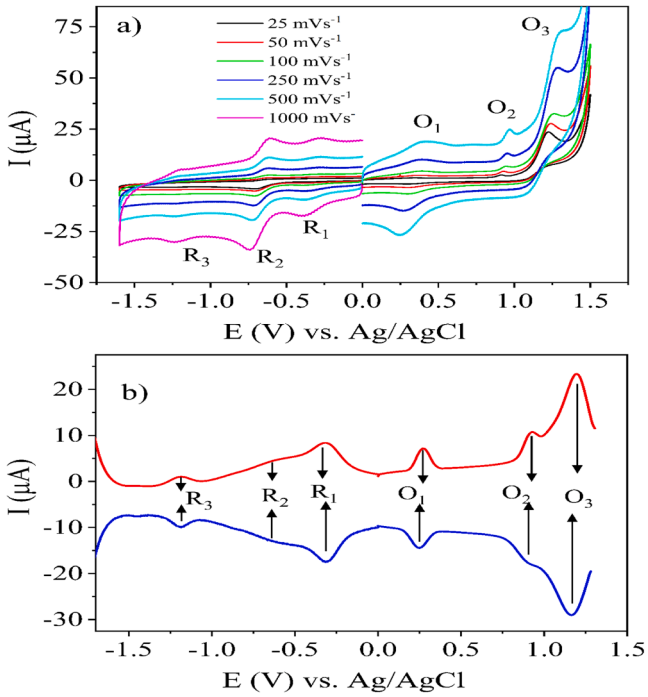

Fig. 5. CVs and SWVs of **nANTH—CoPc** (5.0×10^{-4} mol.dm^{-3}) recorded at various scan rates on a GCE working electrode in DMSO/TBAP.

*2.1.2.3. 1(4),8(11),15(18),22(25)-[4-((1,5-dimethyl-3-oxo-2-phenyl-2,3-dihydro-1H-pyrazol-4-ylimino)methyl)phenoxy)] phthalocyaninato manganese (III)chloride (**nANTH-MnClPc**).* Yields: 30 % (30 mg). Melting point >300 °C. FT–IR (ATR), υ_{max} (cm^{-1}): 3059 (Ar–H), 2923–2853 (Aliph. C–H), 1723, 1646, 1592, 1476, 1355, 1245, 1155, 972, 833. UV–Vis ($CHCl_3$), λ_{max}, nm (logε): 752 (5.06), 682 (4.55), 520 (4.52), 404 (5.17). MS (MALDI–TOF) *m/z*: Calculated: 1824.24; found 1824.59 as $[M]^+$ for $C_{104}H_{76}N_{20}O_8MnCl$.

3. Results and discussion

3.1. All compounds' characterizations

The synthesis route of Schiff base substituted cobalt (**nANTH—CoPc**), copper (**nANTH—CuPc**), and manganese (**nANTH-MnClPc**) phthalocyanines and the phthalonitrile compound (**nANTH—CN**), which is the precursor molecule for these compounds, is given in Scheme 1.

Results from Fouirer Transform Infrared spectroscopy (FT-IR) and nuclear magnetic resonance (NMR) spectroscopy, UV–Vis spectrophotometry, and matrix-assisted laser desorption ıonization–time of flight (MALDI-TOF) mass spectrometry were in agreement with all compounds' theoretical structures, and the experimental section contains all pertinent information.

The structure of the precursor phthalonitrile compound (**nANTH—CN**) is confirmed by the observation of the nitrile stretching vibration at 2231 cm^{-1} in the FT-IR spectrum. This compound's imine group (CH=N) was detected at 9.68 ppm, aromatic protons were detected among 8.09–7.09 ppm, and methyl groups were detected between 3.16 (N—CH_3) ppm and 2.57 (CH_3) ppm in the ^{1}H NMR spectrum. In the ^{13}C NMR spectrum, the imine group (C=N) was seen at 160.09 ppm, and the nitrile groups (C≡N) were seen at 117.76 and 117.51 ppm. (refer to Figs. 1–S1).

Schiff base-substituted precursor phthalonitrile derivative's (**nANTH—CN**) mass spectrum (MALDI-TOF) result verified the molecular ion peak at *m/z* 433.07 as $[M]^+$ (refer to Fig. 2).

The metallated phthalocyanines (**nANTH—Co/Cu/MnClPc**) with 4-

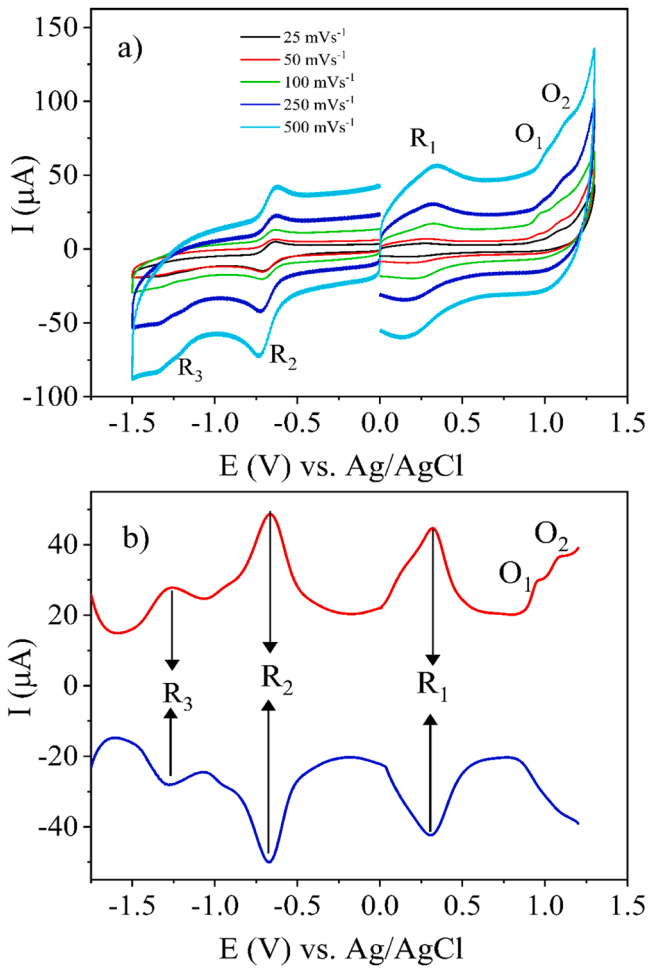

Fig. 6. CVs and SWVs of **nANTH-MnClPc** (5.0×10^{-4} mol.dm^{-3}) recorded at various scan rates on a GCE working electrode in DMSO/TBAP.

((1,5-dimethyl-3-oxo-2-phenyl-2,3-dihydro-1*H*-pyrazol-4-ylimino) methyl)phenoxy) moieties at the non-peripherally tetra substituted and the preferred solvent, n-penthanol at reflux temperature, were produced by cyclotetramerization of the precursor ligand (**nANTH—CN**) in the presence of metal salts ($CoCl_2$, $CuCl_2$, and $MnCl_2$) in an attempt to prepare targeted MPcs.

The disappearance of the strong C≡N vibration at 2231 cm^{-1} indicated the cyclotetramerization of the phthalonitril derivative, and thus the formation of phthalocyanine compounds (**nANTH—Co/Cu/MnClPc**) was observed in the FT-IR. The paramagnetic properties of the Schiff base substituted cobalt (**nANTH—CoPc**), copper (**nANTH—CuPc**), and manganese (**nANTH-MnClPc**) phthalocyanines prevented NMR measurement from being performed. Pcs exhibit two absorption bands in the UV–Vis spectrum, referred to as the Q and B bands, which are among the most significant indicators of phthalocyanine compound synthesis [35]. We measured the UV–Vis spectra of the cobalt (**nANTH—CoPc**), manganese (**nANTH-MnClPc**), and copper (**nANTH—CuPc**) phthalocyanines in $CHCl_3$. These compounds' Q and B bands were measured to be between 752−690 nm and 404−335 nm, respectively. **nANTH-MnClPc** also showed the B band in addition to the new absorption band at about 520 nm (refer to Fig. 3).

The synthesis of Pcs required $MnCl_2$, hence the production of $Mn^{II}Pc$ was expected. On the other hand, the $Mn^{II}Pc$ (**nANTH-MnClPc**) has redshifted Q band absorption in the UV–Vis spectrum. This observation recommended the formation of $Mn^{III}Cl$-type phthalocyanine. The primary cause of the synthesis of the $Mn^{III}ClPc$ product during purification procedures was most likely the aerobic conditions. The **nANTH-MnClPc** UV–Vis spectrum is clearly different from the **nANTH—CoPc** and **nANTH—CuPc** spectra. In the compound with Pc, **nANTH-MnClPc** has an oxidation state of 3+, whereas the oxidation states of **nANTH—CoPc** and **nANTH—CuPc** are 2+. In comparison to the Q bands of the other Pc-Co and Pc-Cu, the Q band of Pc-Mn is displaced by 54–62 nm. Additionally, the **nANTH-MnClPc** UV–Vis spectrum has a red-shifted Q band at 752 nm, which is characteristic of $Mn^{III}ClPc$ [35].

The molecular ion peaks in the phthalocyanines mass spectra were found to be at *m/z* values of 1793.97 as $[M + H]^+$ **nANTH—CoPc**, 1797.85 as $[M]^+$ **nANTH—CuPc**, and 1824.59 as $[M]^+$ **nANTH-MnClPc** (refer to Fig. S2).

3.2. Voltammetric measurements

Especially, the number of electron transfer reactions, ease of the redox processes, and their reversibility are among the fundamental factors for their usage in different electrochemical fields [41–46]. Thus, here the number of redox reactions, redox reaction characters, and influence of the metal centers on the redox richness of the MPcs are determined with cyclic voltammetry (CV) and square wave voltammetry (SWV) measurements on glassy carbon electrode (GCE) indimethyl sulfoxide (DMSO) / tetrabuthlyammonium perchlorrate (TBAP) electrolyte. The half-wave potentials of the redox processes of the complexes were electrochemical analyses derived from the SWVs and the results are tabulated in Table 1. As shown in this table, and Fig. 4, **nANTH—CuPc** illustrates three reductions at −0.63 V (R_1), −1.02 V (R_2), and −1.46 V (R_3), and two oxidation processes 1.02 V (O_1) and −1.43 V (O_2). All reduction reactions have diffusion-controlled and electrochemically reversible character concerning the peak-to-peak separation (ΔE_p), peak current to the square rate of the scan rates (I_p vs. $\nu^{1/2}$), and peak current ratio (I_{pa}/I_{pc}) responses. However, the oxidation couples have quasi-reversible characters [47]. The position of the reduction and oxidation potentials indicate their Pc-based characters and the redox cuples are assigned to $[Cu^{II}Pc^{2-}]/[Cu^{II}Pc^{3-}]^{1-}$ (R_1), $[Cu^{II}Pc^{3-}]^{1-}/[Cu^{II}Pc^{4-}]^{2-}$ (R_2), $[Cu^{II}Pc^{4-}]^{2-}/[Cu^{II}Pc^{5-}]^{3-}$ (R_3), $[Cu^{II}Pc^{2-}]/[Cu^{II}Pc^{1-}]^{1+}$($O_1$), and $[Cu^{II}Pc^{1-}]^{1+}/[Cu^{II}Pc^{0}]^{2+}$($O_2$). Since Redox-active metal centers generally give electron transfer reactions before the Pc based one at low potentials due to the positioning of the d orbitals of the metal center between the highest occupied molecular orbital (HOMO) and the lowest unoccupied molecular orbital (LUMO) of the Pc ring. This is not the case for CuPc since Cu^{2+} is not a redox-active cation when coordinated in the Pc ring [48–50]. As shown in Table 1, **nANTH—CuPc** illustrates similar redox couples at similar potentials with the similar CuPc reported in the literature.

CoPc and MnPc illustrate different redox responses than CuPc due to the redox activity of Co^{2+} and Mn^{3+}central cations. Due to the location of the empty and/or occupied d orbitals of Co^{2+} and Mn^{3+}cations between HOMO and LUMO of the Pc ring, reduction reactions of metal centers are observed before the Pc-based ones, which enhance the redox richness of these complexes [51–54]. As illustrated in Fig. 5, two metal-based processes, $[Co^{II}Pc^{2-}]/[Co^{I}Pc^{2-}]^{1-}$and $[Co^{II}Pc^{2-}]/[Co^{III}Pc^{2-}]^{1+}$couples, are observed at −0.32 V (R_1) and 0.31 V (O_1) respectively. Additionally, Pc-based reductions and oxidations at −0.67 V (R_2) and −1.20 V (R_3), 0.94 V (O_2), and 1.19 V (O_3) are recorded after the metal-based electron transfer reactions. These assignments are in harmony with the similar CoPcs given in Table 1, and they are proved with the *in-situ* spectroelectrochemical measurements discussed below. Concerning ΔE_p, I_p vs. $\nu^{1/2}$, and I_{pa}/I_{pc} responses while the R_1 and O_1 couples are electrochemically and chemically reversible, the other couples have chemically quasi-reversible characters. The reversibility of the redox processes of **nANTH—CoPc** is clearly shown in the SWVs (Fig. 6b).

Fig. 6 illustrates the CVs and SWVs of **nANTH-MnClPc** in the DMSO/TBAP electrolyte. MnPcs undergo three reductions and one oxidation process within the electrolyte potential window. Due to the redox active Cl^{-1}-Mn^{+3} metal center, this complex gives two metal-based reduction

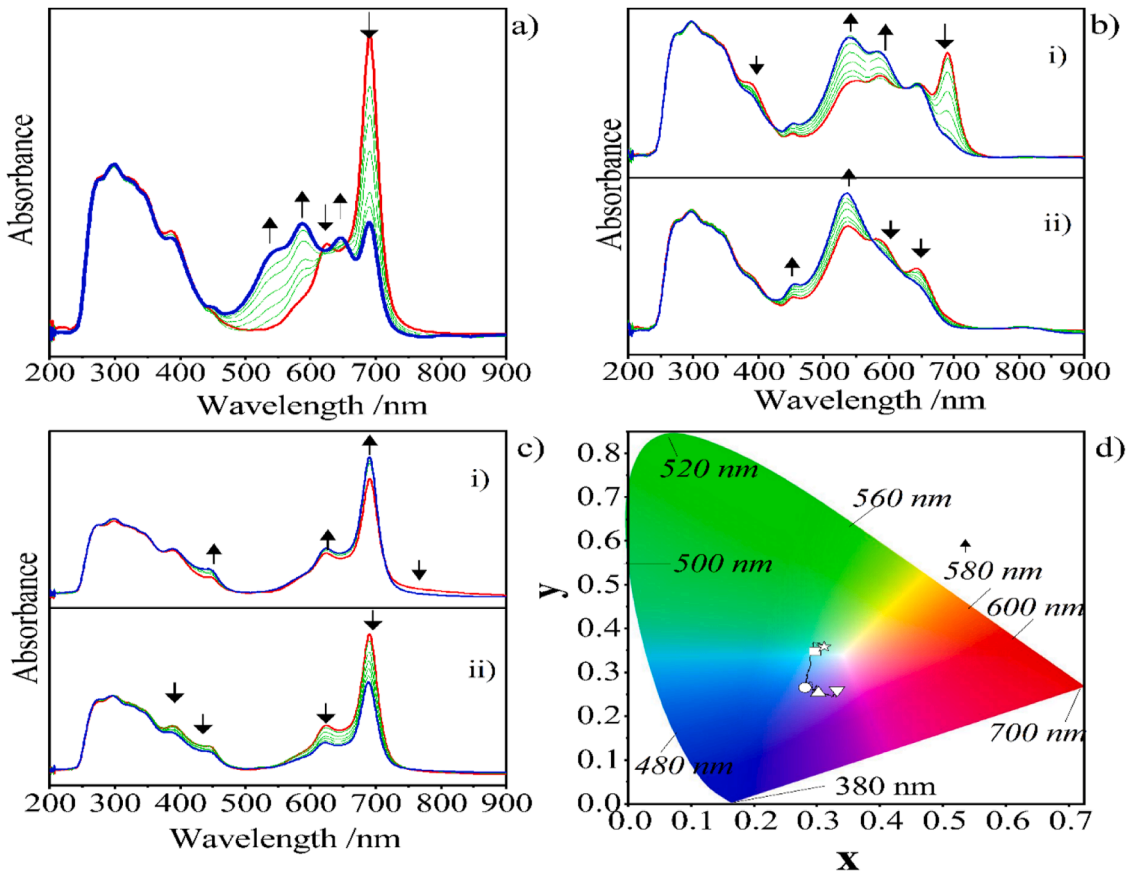

Fig. 7. *In-situ* UV–Vis spectral changes of **nANTH—CuPc** in DMSO/TBAP electrolyte. a) E_{app}= −0.80 V b) i: E_{app}= −1.20 V, ii: E_{app}= −1.60 V, c) i: E_{app}= 1.20 V, ii: E_{app}= 1.50 V, d) Chromaticity diagram (each symbol represents the color of electro-generated species; : $[Cu^{II}Pc^{-2}]$; :$[Cu^{II}Pc^{-3}]^{1-}$; : $[Cu^{II}Pc^{-4}]^{2-}$; : $[Cu^{II}Pc^{-5}]^{3-}$; : $[Cu^{II}Pc^{0}]^{2+}$.

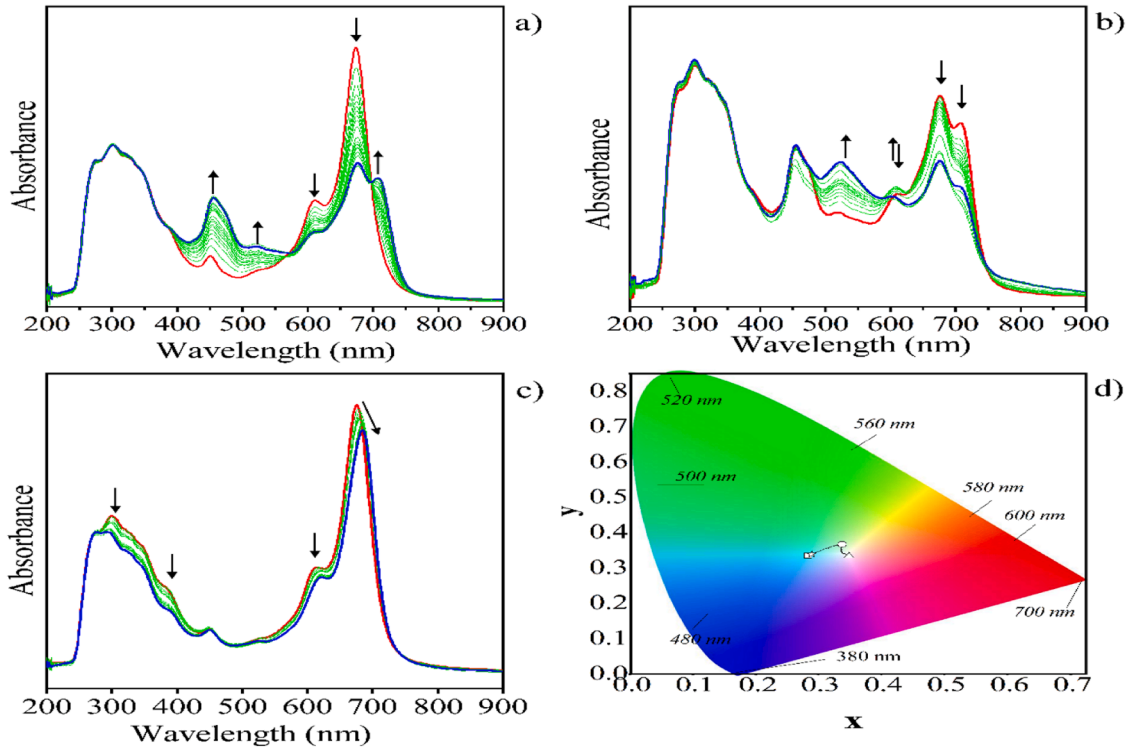

Fig. 8. *In-situ* UV–Vis spectral changes of **nANTH—CoPc** in DMSO/TBAP electrolyte. a) E_{app}= −0.45 V b) E_{app}= −1.20 V, c) E_{app}= 0.50 V, d) Chromaticity diagram (each symbol represents the color of electro-generated species; : $[Co^{II}Pc^{-2}]$; :$[Co^{I}Pc^{-2}]^{1-}$; : $[Co^{II}Pc^{-3}]^{2-}$; : $[Co^{III}Pc^{-2}]^{1+}$.

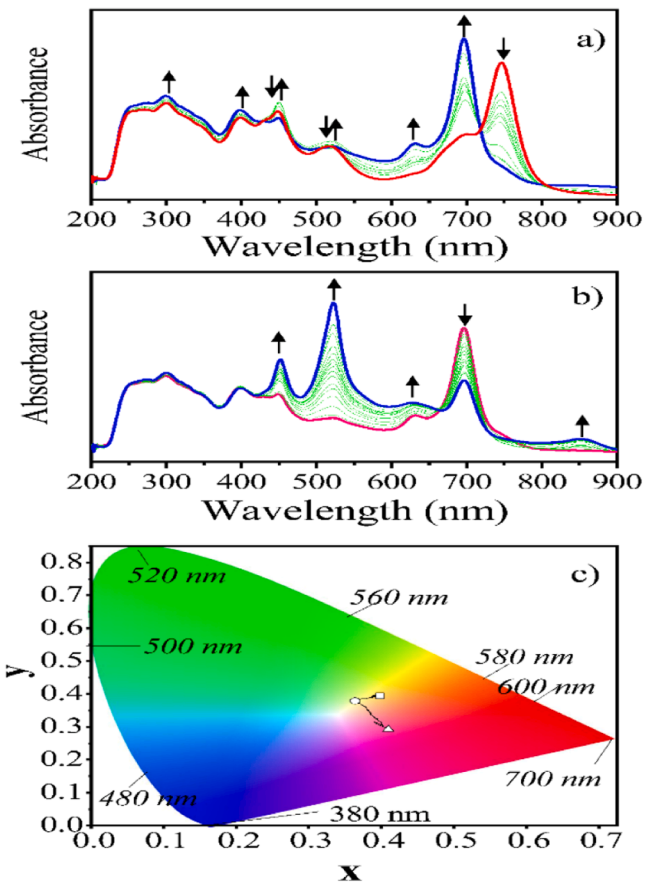

Fig. 9. *In-situ* UV–Vis spectral changes of **nANTH-MnClPc** in DMSO/TBAP electrolyte. a) E_{app}= 0.00 V, b) E_{app}= −0.80 V, c) Chromaticity diagram (each symbol represents the color of electro-generated species; : $[Cl^{1-}\text{-}Mn^{III}Pc^{-2}]$; : $[Cl^{1-}\text{-}Mn^{II}Pc^{-2}]^{1-}$; : $[Cl^{1-}\text{-}Mn^{I}Pc^{-2}]^{2}$.

reactions at 0.24 V (R_1) and −0.67 V (R_2), which are assigned to $[Cl^{1-}\text{-}Mn^{III}Pc^{2-}]/[Cl^{1-}\text{-}Mn^{II}Pc^{2-}]^{1-}$ and $[Cl^{1-}\text{-}Mn^{II}Pc^{2-}]^{1-}/[Cl^{1-}\text{-}Mn^{I}Pc^{2-}]^{2-}$ reductions. Additionally, Pc-based one reduction and two oxidation processes are also observed at −1.25 V (R_2), 0.96 V (O_2), and 1.16 V (O_3), respectively [55,56]. Due to the chemical reaction succeeding the R_2 process, the R_3 couple has a small peak current concerning R_1 and R_2. Also, O_2 and O_3 peaks have small peak potential concerning the O_1 couple due to the succeeding chemical reactions.

3.3. *In-situ spectroelectrochemical measurements*

In-situ spectroelectrochemical measurements (SEC) lor of the electrogenerated species. SEC responses of **nANTH—CuPc** are given in Fig. 7. During the reduction reactions the Q band changes without shifting and new bands are observed in the ligand-to-metal charge transfer. All of these spectral changes are consistence with the Pc-based reduction processes reported in the literature [46,57,58]. While distinct spectral changes are observed during the reduction reactions (Fig. 7a-b), oxidation reactions do not cause distinct spectral changes (Fig. 7c). Significant spectral changes observed during the reduction reactions resulted in significant color change as shown in Fig. 7d. The cyan color of the neutral **nANTH—CuPc** (point : x = 0.2977 and y = 0.3486) changes to blue (point : x = 0.2812 and y = 0.2654), purple (point : x = 0.3029 and y = 0.2529) and then to pink (point : x = 0.3326 and y = 0.2602) after the R_1, R_2 and R_3 couples. A distinct color change is not observed during the oxidation reactions.

CoPc has different SEC responses than that of CuPc due to the metal-based reduction and oxidation of CoPc which gave completely different spectral changes. As shown in Fig. 8a, the Q band of **nANTH—CoPc** shifts from 670 nm to 706 nm, and a new band is observed at 456 nm during the first reduction reaction (R_1) of **nANTH—CoPc** at −0.50 V applied potential, which are characteristic changes for the reduction of $[Co^{II}Pc^{-2}]$ to $[Co^{I}Pc^{-2}]^{1-}$ [46,52,59,60]. The band at 456 nm is the characteristic band of the Co^{1+} oxidation state of the **nANTH—CoPc**. Well-resolved isosbestic points at 570 and 693 nm indicate the chemical reversibility of the process. During the second reduction reaction, observation of a band at 535 nm and decrease of the Q band at 706 nm without a shift are characteristic changes of the reduction of $[Co^{I}Pc^{-2}]^{1-}$ to $[Co^{I}Pc^{-3}]^{-2}$ species (Fig. 8b). Similarly characteristic spectral changes for the $[Co^{II}Pc^{-2}]$ / $[Co^{III}Pc^{-2}]^{1+}$process are observed during the O_1 oxidation couple (Fig. 8c). Shifting of the Q band to longer wavelengths with slight increase in intensity are the indicator of the metal-based oxidation process. The chromaticity diagram in Fig. 8d shows changing the cyan color of the neutral **nANTH—CoPc** (point : x = 0.281 and y = 0.342) of $[Co^{II}Pc^{-2}]$ to green (point : x = 0.334 and y = 0.363) and then light yellow (point : x = 0.350 and y = 0.328) after the R_1 and R_2 processes. A significant color change is not observed after the oxidation reactions as shown in Fig. 8d.

As shown in Fig. 9, SEC responses of **nANTH-MnClPc** support the metal-based reduction characters of the R_1 and R_2 process in the DMSO/TBAP electrolyte. Without a potential application, **nANTH-MnClPc** gives the Q band at longer wavelengths concerning CuPc and CoPc due to the Mn^{3+} oxidation state of the central metal [52,61]. Under 0.0 V applied constant, the Q band shifts from 744 nm to 693 nm (Fig. 9a), which are characteristic chances for the reduction of the $[Cl^{1-}\text{-}Mn^{III}Pc^{2-}]$ to the $[Cl^{1-}\text{-}Mn^{II}Pc^{2-}]^{1-}$ species [46]. The characteristic band for the Mn^{3+} oxidation state at 515 nm disappeared after the R_1 process due to the reduction to the Mn^{3+} oxidation state. During the second reduction reaction at −0.80 V, the characteristic Q bands of $[Cl^{1-}\text{-}Mn^{II}Pc^{2-}]^{1-}$ species at 693 nm decrease in intensity while the characteristic Q band of $[Cl^{1-}\text{-}Mn^{I}Pc^{2-}]^{2-}$ species increase at 518 nm (Fig. 9b) [18]. Moreover, two charge transfer bands are also observed at 452 nm and 851 nm during the R_2 process [41,46,62–64]. No observable spectral change could be recorded during the process. Color changes during the reduction reactions are represented in the chromaticity diagram in Fig. 9c, the orange color of the $[Cl^{1-}\text{-}Mn^{III}Pc^{2-}]$ species (point : x = 0.407 and y = 0.380) turns to green (point : x = 0.410 and y = 0.286), and then dark red color (point : x = 0.320 and y = 0.300) after the reduction reactions.

4. Conclusion

The cobalt (**nANTH—CoPc**), cupper (**nANTH—CuPc**), and manganese (**nANTH-MnClPc**) phthalocyanine substituted with four Schiff base substituents in non-peripheral locations has been synthesized and described successfully. Voltammetric responses supported the proposed structure of the complexes. While **nANTH—CuPc** illustrated only Pc-based redox processes, **nANTH—CoPc** and **nANTH-MnClPc** gave metal-based electron transfer reactions in addition to the Pc-based processes. Enhancement of the redox richness with the incorporation of Co^{2+} and Mn^{3+} central metals to the Pc ring increases the functionality of these complexes in different electrochemical applications. Observation of distinct spectral and color changes during the redox reaction of the complexes indicated their possible functionalities in optoelectronic fields.

CRediT authorship contribution statement

Halise Yalazan: Writing – review & editing, Writing – original draft, Visualization, Validation, Methodology, Investigation, Conceptualization. **Zehra Kurtuluş:** Writing – original draft, Visualization, Validation, Methodology, Investigation, Conceptualization. **Atıf Koca:** Writing – review & editing, Validation, Resources, Methodology, Investigation, Funding acquisition. **Halit Kantekin:** Writing – review & editing, Validation, Supervision, Resources, Investigation, Funding acquisition.

Declaration of competing interest

The authors declare that they have no known competing financial interests or personal relationships that could have appeared to influence the work reported in this paper.

Data availability

The authors do not have permission to share data.

Acknowledgments

Atıf Koca thanks the Turkish Academy of Sciences (TUBA) for its support.

Supplementary materials

Supplementary material associated with this article can be found, in the online version, at doi:10.1016/j.molstruc.2024.139999.

References

[1] M. Falke, X. Graehlert, U. Falke, S. Schulze, M. Hietschold, Structural imaging of lanthanoide diphthalocyanines by transmission electron microscopy, Physica Status Solid (a) 150 (1) (1995) 359–369.
[2] H. De Diesbach, E. von der Weid, Quelques sels complexes des o-dinitriles avec le cuivre et la pyridine, Helv. Chim. Acta 10 (1) (1927) 886–888.
[3] R. Bayrak, S.K. Ataşen, I. Yılmaz, İ. Yalçın, M. Erman, Y. Ünver, İ. Değirmencioğlu, Synthesis and spectro-electrochemical properties of new metallophthalocyanines having high electron transfer capability, J. Mol. Struct. 1231 (2021) 129677.
[4] N.S. Ertunga, E.T. Saka, T. Taskin-Tok, M.Y. Akatin, K.İ. Bektas, A. Colak, Synthesis, characterization, DNA interaction, molecular docking, and α-glucosidase inhibition studies of 3-(pyrimidin-2-ylthio) groups substituted water soluble zinc (II) phthalocyanine, Appl. Organomet. Chem. 38 (2024) e7583.
[5] D. Akkaya, B. Barut, S. Sari, R. Reis, H. Fazli, Z. Biyiklioglu, A. Özel, Synthesis and biological evaluation of novel zinc (II) and nickel (II) phthalocyanines as cholinesterase inhibitors, J. Organomet. Chem. 995 (2023) 122742.
[6] H. Yalazan, A.A. Kamiloglu, A. Tekin, T. Arslan, H. Kantekin, Synthesis and *in vitro* acetylcholinesterase (AChE) and butyrylcholinesterase (BChE) enzymes activity of aldehyde and Schiff base substituted cobalt (II), copper (II), and zinc (II) phthalocyanines, Appl. Organomet. Chem. (2024) e7440.
[7] B.A. Öztürmen, Ç. Akkol, E.T. Saka, Z. Biyiklioglu, Synthesis of water soluble cobalt (II), copper (II) phthalocyanines and their usage as a catalyst in the photoxidation of benzyl alcohol in biphasic catalysis, Inorg. Chem. Commun. 158 (2023) 111647.
[8] M.K. Keşir, Z. Bıyıklıoğlu, Peripherally tetra-substituted zinc (II) phthalocyanine sensitized TiO_2 composite: monitoring with tandem LC/MS and photocatalytic degradation of amoxicillin, J. Organomet. Chem. 1005 (2024) 122969.
[9] H. Yalazan, Ç. Akkol, E.T. Saka, H. Kantekin, Investigation of photocatalytic properties of cobalt phthalocyanines on benzyl alcohol photoxidation, Appl. Organomet. Chem. 37 (2023) e6975.
[10] D. Akyüz, Ü. Demirbaş, Sensor performances of novel piperidine substituted cobalt (II) and copper(II) phthalocyanines for detection of dopamine, ascorbic acid and uric acid, J. Organomet. Chem. 982 (2022) 122537.
[11] D. Akyüz, A. Koca, An electrochemical sensor for the detection of pesticides based on the hybrid of manganese phthalocyanine and polyaniline, Sens. Actuators, B 283 (2019) 848–856.
[12] Ö. Ödemiş, M.S. Ağırtaş, D.G. Solğun, A. Özkartal, Effect of silver nanoparticles prepared by green chemistry on the photovoltaic properties of zinc phthalocyanine, Chem. Pap. 78 (2024) 3735–3746.
[13] A.M. Sevim, S. Çakar, M. Özacar, A. Gül, Electrochemical and photovoltaic properties of highly efficient solar cells with cobalt/zinc phthalocyanine sensitizers, Sol. Energy 160 (2018) 18–24.
[14] İ. Ömeroğlu, A. Şenocak, H. Yetkin, H. Yüksel Güney, E. Demirbaş, M. Durmuş, BODIPY substituted zinc (II) phthalocyanine and its bulk heterojunction application in solar cells, J. Porphyrins Phthalocyanines 23 (2019) 1132–1143.
[15] M. Urbani, M.-E. Ragoussi, M.K. Nazeeruddin, T. Torrres, Phthalocyanines for dye-sensitized solar cells, Coord. Chem. Rev. 381 (2019) 1–64.
[16] B. Kadem, E.N. Kaya, A. Hassan, M. Durmuş, T. Basova, Composite materials of P3HT:PCBM with pyrene substituted zinc(II) phthalocyanines: characterisation and application in organic solar cells, Sol. Energy 189 (2019) 1–7.
[17] İ. Ömeroğlu, M. Durmuş, Water-soluble phthalocyanine photosensitizers for photodynamic therapy, Turk. J. Chem. 47 (2023) 837–863.
[18] H. Yalazan, İ. Ömeroğlu, G. Çelik, H. Kantekin, M. Durmuş, Fluorinated pyrazoline-linked axial silicon phthalocyanine, alpha (α) and beta (β) zinc phthalocyanines on photophysicochemical properties, Inorg. Chim. Acta 551 (2023) 121480.
[19] Ö. Güleç, A.T. Bilgiçli, C. Hepokur, A. Günsel, M. Arslan, M.N. Yarasir, Novel and effective peripheral tetra-substituted phthalocyanines with quinazoline groups for cancer treatment: synthesis, photophysical and photochemical properties, and *in-vitro* studies, J. Photochem. Photobiol., A 452 (2024) 115587.
[20] C.G. Claessens, U. Hahn, T. Torres, Phthalocyanines: from outstanding electronic properties to emerging applications, Chem. Record 8 (2008) 75–97.
[21] P. Gregory, Industrial applications of phthalocyanines, J. Porphyrins Phthalocyanines 4 (2012) 432–437.
[22] G. de la Torre, G. Bottari, U. Hahn, T. Torres, Functional phthalocyanines: synthesis, nanostructuration, and electro-optical applications, Functional Phthalocyanine Molecular Materials 135 (2010) 1–44.
[23] S. Yang, Y. Yu, X. Gao, Z. Zhang, F. Wang, Recent advances in electrocatalysis with phthalocyanines, Chem. Soc. Rev. 50 (2021) 12985–13011.
[24] E. Demir, H. Silah, B. Uslu, Phthalocyanine modified electrodes in electrochemical analysis, Crit. Rev. Anal. Chem. 52 (2022) 425–461.
[25] K. Kadish, R. Guilard, K.M. Smith, The Porphyrin Handbook: Phthalocyanines: Spectroscopic and Electrochemical Characterization, Academic Press, 2012.
[26] A. Nas, Z. Biyiklioglu, S. Fandaklı, G. Sarkı, H. Yalazan, H. Kantekin, Tetra(3-(1,5-diphenyl-4,5-dihydro-1H-pyrazol-3-yl)phenoxy) substituted cobalt, iron and manganese phthalocyanines: synthesis and electrochemical analysis, Inorg. Chim. Acta 466 (2017) 86–92.
[27] Ü. Demirbaş, D. Akyüz, H.T. Akçay, A. Koca, E. Menteşe, H. Kantekin, Novel 1,2,4-triazole substituted metallo-phthalocyanines: synthesis, characterization and investigation of electrochemical and spectroelectrochemical properties, J. Mol. Struct. 1173 (2018) 205–212.
[28] N. Kobayashi, Synthesis and spectroelectrochemistry ofnew phthalocyanines with ester functionalities, Dyes Pigm. 92 (2012) 1114.
[29] A.M. Sevim, S. Arıkan, A. Koca, A. Gül, Synthesis and spectroelectrochemistry ofnew phthalocyanines with ester functionalities, Dyes Pigm. 92 (2012) 1114.
[30] O. Dolotova, A. Konarev, K. Volkov, V. Negrimovsky, O.L. Kaliya, Coordinationand electrochemistry of new substituted manganese phthalocyanines, J. Porphyrins Phthalocyanines 16 (2012) 946.
[31] I.A. Akinbulu, K.I. Ozoemena, T. Nyokong, Formation, surface characterization, and electrocatalytic application of self-assembled monolayer films of tetra-substituted manganese, iron, and cobalt benzylthio phthalocyanine complexes, J. Solid State Electrochem. 15 (2011) 2239.
[32] S. Altun, Z. Odabaş, A. Altındal, A.R. Özkaya, Coumarin-substituted manganese phthalocyanines: synthesis, characterization, photovoltaic behaviour, spectral and electrochemical properties, Dalton Trans. 43 (2014) 7987–7997.
[33] I.A. Akinbulu, T. Nyokong, The effects of point of substitution on the electrochemical behavior of new manganese phthalocyanines, tetra-substituted with diethylaminoethanethiol, Inorg. Chim. Acta 363 (2010) 3229–3237.
[34] H. Yalazan, Y.E. Maden, A. Koca, H. Kantekin, Multi-step syntheses, electrochemistry and spectroelectrochemistry of peripheral Co^{II}, Cu^{II} and $Mn^{III}Cl$ phthalocyanines bearing pyrazoline, J. Mol. Struct. 1269 (2022) 133788.
[35] H. Yalazan, H. Kantekin, Ö. Budak, A. Koca, Non-peripheral tetra methoxylated pyrazoline bearing Co^{II}, Cu^{II} and $Mn^{III}Cl$ phthalocyanines: syntheses, electrochemistry and spectroelectrochemistry, J. Organomet. Chem. 973-974 (2022) 122405.
[36] Koca, A. (2016). Spectroelectrochemistry of phthalocyanines. Electrochemistry of N4 macrocyclic metal complexes: volume 2: biomimesis, electroanalysis and electrosynthesis of MN4 metal complexes, 135–200.
[37] K. Harmandar, M.F. Saglam, I.F. Sengul, G. Ekineker, P. Balcik-Ercin, M. Göksel, D. Atilla, Novel triazole containing zinc (II)phthalocyanine Schiff bases: determination of photophysical and photochemical properties for photodynamic cancer therapy, Inorg. Chim. Acta 519 (2021) 120286.
[38] J. Obirai, T. Nyokong, Synthesis, spectral and electrochemical characterization of mercaptopyrimidine-substituted cobalt, manganese and Zn (II) phthalocyanine complexes, Electrochim. Acta 50 (2005) 3296–3304.
[39] G. Kuntoji, N. Kousar, S. Gaddimath, L Koodlur Sannegowda, Macromolecule–nanoparticle-based hybrid materials for biosensor applications, Biosensors 14 (2024) 277.
[40] O.A. Hamad, R.O. Kareem, P.K. Omer, Properties, characterization, and application of phthalocyanine and metal phthalocyanine, J. Chem. Rev. 6 (1) (2024) 39–75.
[41] J. Obirai, T. Nyokong, Synthesis, spectral and electrochemical characterization of mercaptopyrimidine-substituted cobalt, manganese and Zn (II) phthalocyanine complexes, Electrochim. Acta 50 (2005) 3296–3304.
[42] G. Mbambisa, P. Tau, E. Antunes, T. Nyokong, Synthesis and electrochemical properties of purple manganese (III) and red titanium (IV) phthalocyanine complexes octa-substituted at non-peripheral positions with pentylthio groups, Polyhedron 26 (2007) 5355–5364.
[43] A. Koca, A.R. Özkaya, M. Selçukoğlu, E. Hamuryudan, Electrochemical and spectroelectrochemical characterization of the phthalocyanines with pentafluorobenzyloxy substituents, Electrochim. Acta 52 (2007) 2683–2690.
[44] J. Obirai, N.P. Rodrigues, F. Bedioui, T. Nyokong, Synthesis, spectral and electrochemical properties of a new family of pyrrole substituted cobalt, iron, manganese, nickel and zinc phthalocyanine complexes, J. Porphyrins Phthalocyanines 7 (2003) 508–520.
[45] M. L'her, A. Pondaven, Electrochemistry of 104, The Porphyrin Handbook, (2003) 117.
[46] A. Koca, Spectroelectrochemistry of Phthalocyanines, Electrochemistry of N4 Macrocyclic Metal Complexes, Springer, 2016, pp. 135–200.
[47] A.J. Bard, L.R. Faulkner, H.S. White, Electrochemical Methods: Fundamentals and Applications, John Wiley & Sons, 2022.
[48] N. Zharnikova, N. Usol'tseva, E. Kudrik, M. Thelakkat, Synthesis, mesomorphism and electrochemical properties of tetrasubstituted zinc and copper phthalocyanines, J. Mater. Chem. 19 (2009) 3161–3167.

[49] A.A. Esenpınar, A.R. Özkaya, M. Bulut, Synthesis and electrochemical properties of crown ether functionalized coumarin substituted cobalt and copper phthalocyanines, J. Organomet. Chem. 696 (2011) 3873–3881.
[50] E. Güzel, A. Koca, A. Gül, M.B. Koçak, Microwave-assisted synthesis, electrochemistry and spectroelectrochemistry of amphiphilic phthalocyanines, Synth. Met. 199 (2015) 372–380.
[51] H.Z. Uzunmehmetoğlu, H.Y. Yenilmez, K. Kaya, A. Koca, A. Altındal, Z.A. Bayır, Electrochemical, spectroelectrochemical, and dielectric properties of metallophthalocyanines bearing redox active cobalt and manganese metal centres, Inorg. Chim. Acta 459 (2017) 51–62.
[52] A. Koca, Spectroelectrochemistry of phthalocyanines, electrochemistry of N4 macrocyclic metal complexes: volume 2: biomimesis, electroanalysis and electrosynthesis of MN4 metal complexes, (2016) 135–200.
[53] M. Peterson, C. Hunt, Z. Wang, S.E. Heinrich, G. Wu, G. Ménard, Synthesis, characterization, and electrochemical properties of a first-row metal phthalocyanine series, Dalton Trans. 49 (2020) 16268–16277.
[54] F. Bedioui, S. Griveau, T. Nyokong, A.J. Appleby, C.A. Caro, M. Gulppi, G. Ochoa, J.H. Zagal, Tuning the redox properties of metalloporphyrin-and metallophthalocyanine-based molecular electrodes for the highest electrocatalytic activity in the oxidation of thiols, Phys. Chem. Chem. Phys. 9 (2007) 3383–3396.
[55] A. Lever, P. Minor, J. Wilshire, Electrochemistry of manganese phthalocyanine in nonaqueous media, Inorg. Chem. 20 (1981) 2550–2553.
[56] A. Lever, P. Minor, Electrochemistry of main-group phthalocyanines, Inorg. Chem. 20 (1981) 4015–4017.
[57] S. Arslan, I. Yilmaz, Preparation, electrochemical, and spectroelectrochemical characterization of a new water-soluble copper phthalocyanine, Inorg. Chem. Commun. 10 (2007) 385–388.
[58] E.T. Saka, G. Sarkı, H. Kantekin, A. Koca, Electrochemical, spectroelectrochemical and catalytical properties of new Cu (II) and Co (II) phthalocyanines, Synth. Met. 214 (2016) 82–91.
[59] W. Nevin, W. Liu, M. Melnik, A. Lever, Spectro-electrochemistry of cobalt and iron tetrasulphonated phthalocyanines, J. Electroanal. Chem. Interfacial Electrochem. 213 (1986) 217–234.
[60] A. Alemdar, A.R. Özkaya, M. Bulut, Synthesis, spectroscopy, electrochemistry and *in situ* spectroelectrochemistry of partly halogenated coumarin phthalonitrile and corresponding metal-free, cobalt and zinc phthalocyanines, Polyhedron 28 (2009) 3788–3796.
[61] C.-L. Lin, C.-C. Lee, K.-C. Ho, Spectroelectrochemical studies of manganese phthalocyanine thin films for applications in electrochromic devices, J. Electroanal. Chem. 524 (2002) 81–89.
[62] D. Quinton, E. Antunes, S. Griveau, T. Nyokong, F. Bedioui, Cyclic voltammetry and spectroelectrochemistry of a novel manganese phthalocyanine substituted with hexynyl groups, Inorg. Chem. Commun. 14 (2011) 330–332.
[63] A.M. Sevim, H.Y. Yenilmez, M. Aydemir, A. Koca, Z.A. Bayır, Synthesis, electrochemical and spectroelectrochemical properties of novel phthalocyanine complexes of manganese, titanium and indium, Electrochim. Acta 137 (2014) 602–615.
[64] İ. Özçeşmeci, A. Koca, A. Gül, Synthesis and electrochemical and *in situ* spectroelectrochemical characterization of manganese, vanadyl, and cobalt phthalocyanines with 2-naphthoxy substituents, Electrochim. Acta 56 (2011) 5102–5114.
[65] D. Akyüz, T. Keleş, Z. Biyiklioglu, A. Koca, Electrochemical pesticide sensors based on electropolymerized metallophthalocyanines, J. Electroanal. Chem. 804 (2017) 53–63.
[66] J. Obirai, T. Nyokong, Synthesis, spectral and electrochemical characterization of mercaptopyrimidine-substituted cobalt, manganese and Zn (II) phthalocyanine complexes, Electrochim. Acta 50 (2005) 3296–3304.
[67] M. Arıcı, D. Arıcan, A.L. Uğur, A. Erdoğmuş, A. Koca, Electrochemical and spectroelectrochemical characterization of newly synthesized manganese, cobalt, iron and copper phthalocyanines, Electrochim. Acta 87 (2013) 554–566.
[68] B. Agboola, K.I. Ozoemena, P. Westbroek, T. Nyokong, Synthesis and electrochemical properties of benzyl-mercapto and dodecyl-mercapto tetrasubstituted manganese phthalocyanine complexes, Electrochim. Acta 52 (2007) 2520–2526.
[69] Ü.E. Özen, T. Keleş, Z. Bıyıklıoğlu, A. Koca, A.R. Özkaya, Electropolymerization and electrochemical pesticide sensor application of metallophthalocyanines bearing polymerizable morpholin groups, J. Electrochem. Soc. 163 (2016) B673–B682.